$^{39}Ar/^{40}Ar$ Ages from the Yozgat Batholith: Preliminary Data on the Timing of Late Cretaceous Extension in the Central Anatolian Crystalline Complex, Turkey

Veysel Isik, Ching-Hua Lo,[1] Cemal Göncüoğlu,[2] and Serhat Demirel[3]

Ankara University, Faculty of Engineering, Department of Geological Engineering, Tectonics Research Group, TR-06100 Ankara, Turkey (e-mail: isik@eng.ankara.edu.tr)

ABSTRACT

Isotopic dating of sheared and unsheared rocks can be important in understanding deformational processes in orogenic belts. This study examines $^{40}Ar/^{39}Ar$ dating of granitoids and mylonitic rocks to constrain intrusive and deformational events within the northern part of the central Anatolian crystalline complex (CACC). The Kerkenez granitoid within this complex, comprising primarily quartz monzonite and hornblende granite, contains discrete ductile shear zones. These zones are characterized by protomylonite and mylonite formations with metamorphism conditions that reach lower amphibolite facies, mylonitic foliations and lineations, and asymmetric kinematic indicators (e.g., asymmetric porphyroclasts, composite shear bands) with top-to-the-northwest shear senses. Considering the high closure temperatures (~500°C for hornblende and ~350°C for K-feldspar), both hornblende quartz monzonite and hornblende granite in the Kerkenez granitoid may have cooled rapidly, suggesting that hornblende quartz monzonite may have been emplaced at around 81.2 ± 0.5 Ma and that it is older than hornblende granite, which has a well-defined plateau age (72.6 ± 0.2 Ma). On the basis of intrusive relations and our $^{40}Ar/^{39}Ar$ age data, we can constrain the upper age limit (~81 Ma) on the regional metamorphism in the northern part of the CACC. The $^{40}Ar/^{39}Ar$ dating of hornblendes in two mylonite samples from a ductile shear zone yields plateau ages of 71.6 ± 0.3 and 71.7 ± 0.2 Ma, respectively. K-feldspars in the same samples yield plateau ages of 71.6 ± 0.2 and 81.3 ± 0.2 Ma. Therefore, we adopt 71.6 ± 0.3 and 71.7 ± 0.2 Ma as the cooling ages of hornblende and K-feldspar, respectively, in the ductile shear zone. On the other hand, an age of 81.3 ± 0.2 Ma for deformed K-feldspar appears to reflect not the age of ductile deformation but rather the age of undeformed hornblende quartz monzonite. These age data suggest that the shear zones formed soon after the emplacement and cooling of hornblende granite. The cooling event of the shear zones is interpreted to be associated with the beginning of extension in the region. Furthermore, these data imply that metamorphism, emplacement, and cooling of the intrusives and ductile shearing of the intrusions were coeval in the region and occurred in the Late Cretaceous.

Online enhancement: appendix table.

Introduction

The Alpine orogeny was the result of the closure of the Neo-Tethys Ocean, the collision of Laurasia and Gondwanaland, and the deformation of their margins since the Late Cretaceous. Turkey is part of the Alpine-Himalayan chain, which is characterized by the presence of several major continental fragments and suture zones that formed as a result of the closure of different branches of the Neo-Tethys Ocean during Late Cretaceous–Miocene time (fig. 1*a*; e.g., Şengör and Yılmaz 1981; Robertson and Dixon 1984; Poisson 1986; Okay and Tüysüz 1999). The İzmir-Ankara-Erzincan (IAE) suture, extending about 2000 km, is the major suture separating the Pontides from the Anatolide-Tauride platform (fig. 1*a*). While the Pontides display Laurasian affinities, the Anatolide-Tauride platform is attributed to the northern margin of Gondwanaland (Şengör and Yılmaz 1981; Okay and Tüysüz 1999). The Kırşehir block is the region surrounded by the IAE suture in the north and the controversial Inner Tauride suture in the south (fig. 1*a*). The block

Manuscript received November 26, 2007; accepted April 29, 2008.

[1] Department of Geosciences, National Taiwan University, 106 Taipei, Taiwan.

[2] Department of Geological Engineering, Middle East Technical University, TR-06531 Ankara, Turkey.

[3] Türkiye Kömür İşletmeleri, TR-06531 Ankara, Turkey.

[The Journal of Geology, 2008, volume 116, p. 510–526] 0022-1376/2008/11605-0006$15.00 DOI: 10.1086/590922

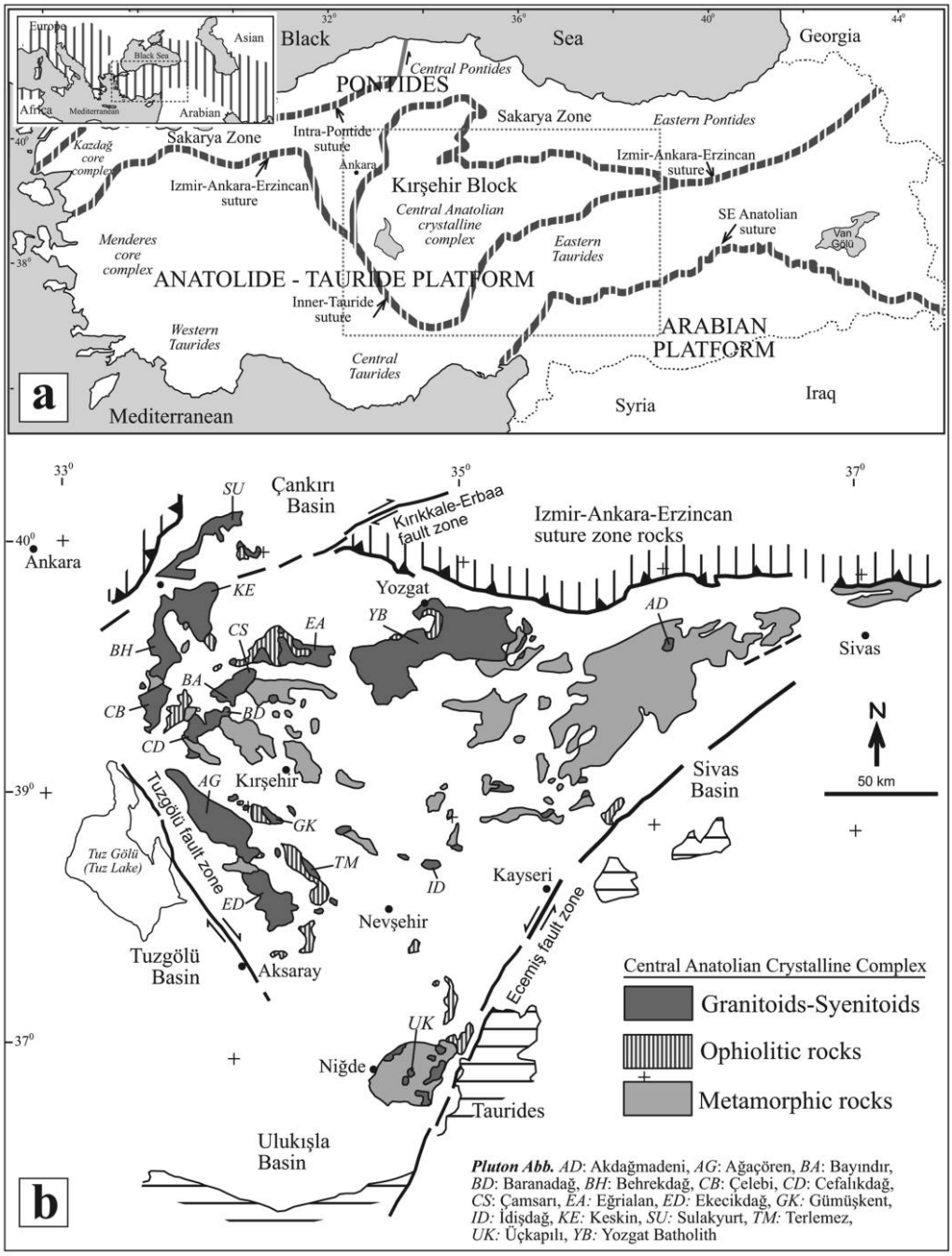

Figure 1. *a*, Map showing major tectonic elements of Turkey. Striped lines represent suture zones (modified from Okay and Tüysüz 1999). Inset map displays area of the Alpine orogeny covering Turkey and its surroundings. *b*, Simplified geologic map of central Turkey, showing distribution of major rock units in the central Anatolian crystalline complex.

consists of massifs (Kırşehir, Akdağ, and Niğde) that are widely referred to as the central Anatolian crystalline complex (CACC) and basins (fig. 1*b*).

The CACC includes Late Cretaceous intensive magmatic rocks that have been the subject of many investigations for the past 3 decades; the petrography, geochemistry, age, and tectonic setting of these intrusives have been discussed (e.g., Şengör and Yılmaz 1981; Tüysüz et al. 1995; Erler and Göncüoğlu 1996; Göncüoğlu et al. 1997; Whitney and Dilek 1997; Boztuğ 2000; Fayon et al. 2001; Kadıoğlu et al. 2003; Boztuğ et al. 2004; Köksal et al.

2004; Whitney et al. 2004; Tatar and Boztuğ 2005). Although there is not yet a consensus on the petrogenesis, age, and geodynamic interpretation of these intrusives, the evidence provided by these studies indicates that (1) the CACC contains diverse magmatism that varies from peraluminous and metaluminous to alkaline/peralkaline; (2) the complex includes many plutons with granitoid and syenitoid components; (3) these plutons are products of either syncollisional to postcollisional magmatism or arc magmatism; and (4) the age of the granitoids is Late Cretaceous, Late Cretaceous–Early Eocene, Paleocene-Eocene, and Miocene (for details, see table 1).

Within the Yozgat batholith (YB), some workers have examined petrographical and geochemical features, and a variety of geochemical interpretations has been presented (e.g., Erler and Göncüoğlu 1996; Boztuğ 2000). The studies suggest the presence of S- and I-type syn- and postcollisional granitoids. In particular, geochronological data from the granitoids within the northern part of the CACC lack constraints for not only the emplacement ages of the granitoids but also the ages of the mylonitic deformational events related to the postcollisional uplift and exhumation.

The dating of minerals using the $^{40}Ar/^{39}Ar$ method is a commonly used technique to date crystallization and deformation and to determine thermochronology (e.g., Foster et al. 1992; Kohn et al. 1997; Bingen et al. 1998; Fossen and Dunlap 1998; Lips et al. 1998; Zegers et al. 1999; Wang and Lu 2000; Xu et al. 2000; Reddy et al. 2001; Isik et al. 2004; Jourdan et al. 2004; Wang et al. 2007). The closure temperature for argon in hornblende and K-feldspar shows a down-temperature progression (500°C for hornblende and 350°C for K-feldspar; e.g., McDougall and Harrison 1988), so analyses of hornblende yield consistently older ages because of its higher closure temperature. On the other hand, K-feldspars are analyzed to study their low-temperature cooling history (e.g., Reddy et al. 2001). The $^{40}Ar/^{39}Ar$ geochronology can also be used to determine the time of mylonitic deformation (e.g.,

Table 1. Previous Geochronology Data from Granitoids/Syenitoids of the Central Anatolian Crystalline Complex

Pluton (map code) and rock unit	Age (Ma)	Method	Reference
Ağaçören (AG):			
Granite	110 ± 14	Rb-Sr (whole rock)	Güleç 1994
Granite	77.6 ± .3	Ar-Ar (biotite)	Kadıoğlu et al. 2003
Gabro	78.6 ± .3	Ar-Ar (amphibol)	
Baranadağ (BD):			
Quartz monzonite	54	Total Pb (zircon)	Ayan 1963
Quartz monzonite	74.0 ± 2.8	U-Pb (titanite)	Köksal et al. 2004
Monzonite	76.4 ± 1.3	K-Ar (hornblende)	İlbeyli et al. 2004
Bayındır (BA):			
Quartz syenite	85.1 ± 3.6	Rb-Sr (whole rock)	Kuruç 1990
Sodalite syenite	84.4 ± .9	Rb-Sr (whole rock)	
Miaskite	71.8 ± .1	Rb-Sr (whole rock)	
Foyaites and volcanites	70.5 ± 3.4	Rb-Sr (whole rock)	
Behrekdağ (BD):			
Leucogranite	69.1 ± 1.42–71.5 ± 1.45	K-Ar (biotite)	Tatar et al. 2003
Quartz monzonite	68.8 ± 1.43–81.2 ± 3.36	K-Ar (hornblende)	
Granite	79.5 ± 1.7	K-Ar (hornblende)	İlbeyli et al. 2004
Cefalıkdağ (CD):			
Granite, granodiorite	71 ± 1.1	Rb-Sr (whole rock, biotite)	Ataman 1972
Quartz monzonite	66.6 ± 1.2	K-Ar (biotite)	İlbeyli et al. 2004
Çamsarı (CS):			
Quartz syenite	74.1 ± .7	U-Pb (titanite)	Köksal et al. 2004
Terlemez (TM):			
Quartz monzonite	67.1 ± 1.3–70.1 ± 1.5	K-Ar (K-feldspar)	Yalınız et al. 1999
Quartz monzonite	81.5 ± 1.9	K-Ar (amphibol)	
Üçkapılı (UK):			
Granodiorite	95 ± 11	Rb-Sr (whole rock)	Göncüoğlu 1986
Granodiorite	78.5 ± 1.2	K-Ar (muscovite)	
Granodiorite	74.9 ± 1–77.9 ± 1.2	K-Ar (biotite)	
Granite	13.7–20	U-Pb (monozite)	Whitney and Dilek 1997
Granite	92–85	U-Pb (zircon)	Whitney et al. 2003
Granite	79.4	Ar-Ar (biotite)	

West and Lux 1993). Although K-feldspars coupled with complex systematic argon can make them ill suited for dating most deformational fabrics (Harrison et al. 1991; West and Lux 1993), hornblendes display quite reliable results for deformational events (Harrison 1981).

With this study, we present the first hornblende and K-feldspar $^{40}Ar/^{39}Ar$ data from the granitoids and a mylonitic shear zone developed within the YB. The results will provide insight into the timing of the tectonic regime that followed the posttectonic magmatism event in central Turkey.

Geological Setting

The CACC is tectonically overlain by rocks of the IAE suture zone, which is a remnant of the northern branch of the Neo-Tethys Ocean and the Çankırı Basin on its northern border. The Tuzgölü Basin is located on the western border, and the Sivas Basin and rocks of the Tauride belt are on the east and south/southeastern borders, respectively. The Ulukışla Basin is located on the southern/southwestern sides of the CACC. Lithologically, the CACC is divided into three broad groups: (1) a metamorphic unit, (2) an ophiolitic mélange unit, and (3) an intrusive unit. All of these units are covered by the sedimentary and volcanic rocks of Cenozoic basins known as the central Anatolian basins (fig. 1*b*).

Metamorphic rocks in the CACC have been described in many studies, and they appear to have similar metamorphic and sequential characteristics. The lower part of the metamorphites contains mainly gneisses and schists, while the upper part consists of schists, amphibolites, marbles, and quartzites. The uppermost part is predominantly marbles, resembling the Mesozoic carbonates of the Anatolide-Tauride platform. Metamorphism ranges in grade from greenschist facies to upper amphibolite and granulite facies with different pressure-temperature-time events during Paleozoic to Tertiary times (e.g., Seymen 1981; Göncüoğlu 1986; Whitney et al. 2001, 2003; Whitney and Hamilton 2004).

The metamorphic rocks are tectonically overlain by ophiolitic rocks, termed the central Anatolian ophiolites by Göncüoğlu et al. (1991). The ophiolitic rocks in the CACC are of suprasubduction zone type, related to an ensimatic arc (e.g., Yalınız et al. 1996), and they represent the remnants of the northern Neo-Tethys Ocean (Şengör and Yılmaz 1981). They are found as either dismembered ophiolite bodies or fragments of various sizes in an ophiolitic mélange that was formed in front of the emplaced ophiolite nappes (Göncüoğlu et al. 1991). The Late Cretaceous (Middle Turonian–Early Santonian) limestone intercalated with pillow lavas of the ophiolitic mélange constrains the age of the ophiolitic rocks (Yalınız and Göncüoğlu 1998).

Varied granitoid/syenitoid plutons in the CACC intruded the metamorphic and ophiolitic units. They form a significant portion of the CACC. The largest of the granitoids lies along the northern and western parts of the CACC (fig. 1*b*). In addition to these granitoid bodies, smaller intrusive bodies occur throughout the area of the CACC. Compositionally, they are calc-alkaline and alkaline and range from monzodiorite to monzonite/granodiorite to granite/syenite (e.g., Akıman et al. 1993; Erler and Göncüoğlu 1996; Aydın et al. 1998; Boztuğ 1998; Kadıoğlu et al. 2003; İlbeyli et al. 2004). The age data in the granitoids and syenitoids, based on different isotopic dating methods performed on granitoid/syenitoid rocks in the CACC, range from 110 to 54 Ma, as listed in table 1. The available ages are mainly from granitoids/syenitoids exposed at the western and southern parts of the CACC, and limited isotopic age data are available from granitoids in the northern part of the CACC.

These units are covered with deposits of numerous basins formed during Late Cretaceous–Tertiary time in central Turkey (e.g., Görür et al. 1984, 1998; Erdoğan et al. 1996; Poisson et al. 1996; Dirik et al. 1999; Gürer and Aldanmaz 2002; Clark and Robertson 2005), observed mainly on the margins of the CACC. The formation and regional tectonic evaluation of these basins have been discussed in several articles, in which different evolutionary models for each basin have been proposed. According to Gürer and Aldanmaz (2002), all the Late Cretaceous–Tertiary basins are of the same origin and developed in postcollisional environments following the closure of the northern Neo-Tethys Ocean.

Yozgat Batholith and Study Area

The YB lies along the northern edge of the CACC in central Turkey and forms the largest pluton within the CACC (fig. 1*b*). It trends west-southwest/east-northwest and includes several intrusive units. The first extensive geological study in the YB and the surrounding area was by Ketin (1955). Erler and Göncüoğlu (1996) subdivided the YB into eight mappable subunits based on structural and textural-mineralogical features and their boundary relationships (fig. 2*a*); these are the Yerköy-Şefeatli, Yozgat, Kerkenez, Karlıtepe, Gelingüllü, Sivritepe, Ocaklı, and Mugallı subunits. The batholith is characterized by felsic and mafic rocks composed of

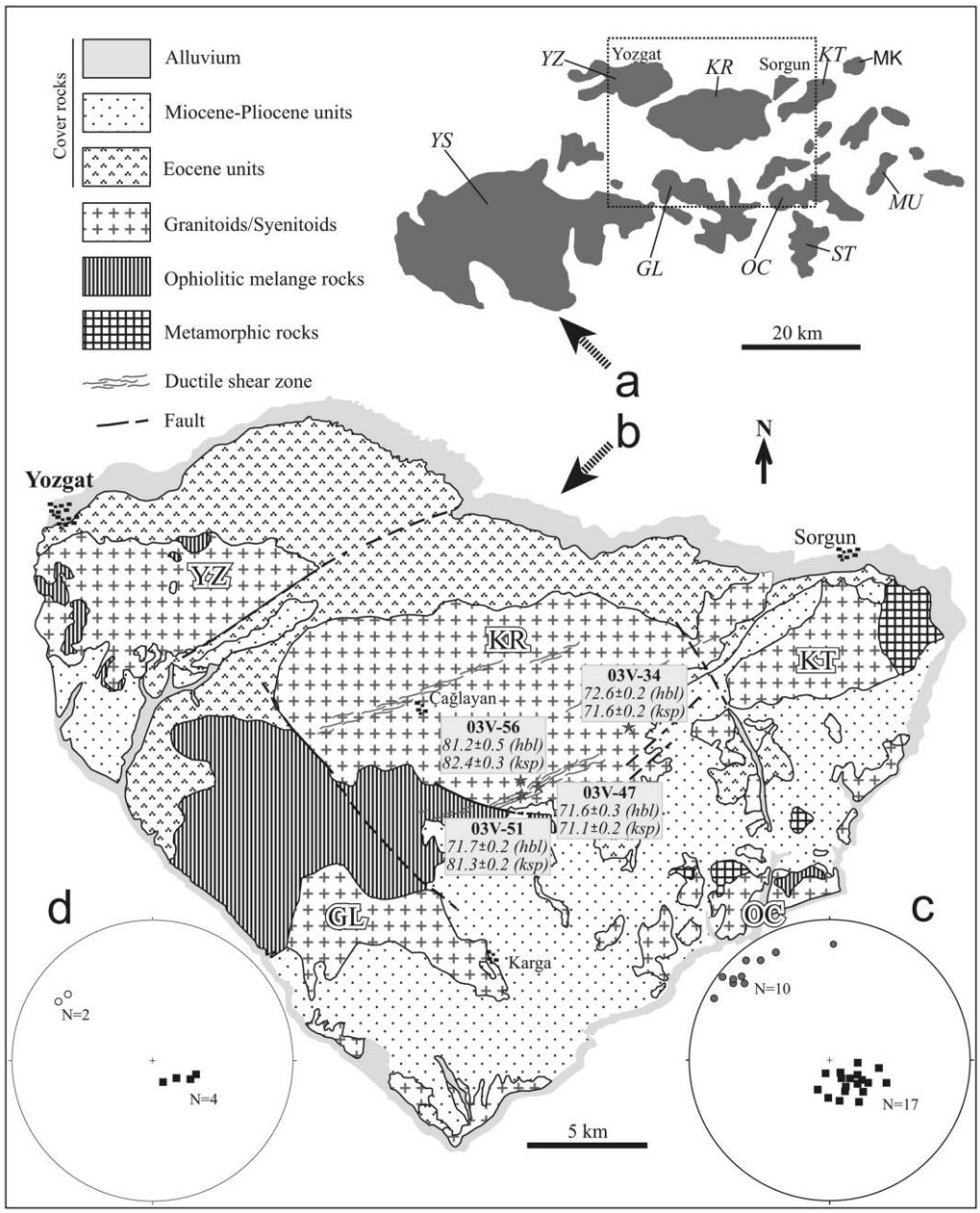

Figure 2. *a*, Index map for figure 1*a*, showing subunits in the Yozgat batholith. *GL* = Gelingüllü, *KT* = Karlıtepe, *KR* = Kerkenez, *MU* = Mugallı, *OC* = Ocaklı, *ST* = Sivritepe, *YS* = Yerköy-Şefeatli, *YZ* = Yozgat. *b*, Simplified geologic map of the study area and its surroundings. The stars show the locations of the samples. *c*, Equal-area, lower-hemisphere projection of stretching lineations (*circles*) and poles of mylonitic foliation (*squares*) in the shear zone exposed in the Kerkenez granitoid. *d*, Equal-area, lower-hemisphere projection of stretching lineations (*circles*) and poles of mylonitic foliation (*squares*) in the shear zone measured in the mélange.

mainly monzogranite, quartz monzonite, granite, granodiorite, tonalite, syenite, and diorite (Ketin 1955; Boztuğ 1995; Erdoğan et al. 1996; Erler and Göncüoğlu 1996; Tatar and Boztuğ 1998). Geochemical data with tectonic discrimination diagrams for rocks of the YB suggest S-type syncollisional, I-type postcollisional, and M-type postcollisional granitoids (e.g., Boztuğ 1995; Erdoğan et al. 1996; Erler and Göncüoğlu 1996; Tatar and Boztuğ 1998). According to Boztuğ (2000), the YB formed either by tectonically overthickened orogenic crust of central Anatolia as a product of syncollisional granitic melts or as alkaline rocks formed by lithospheric extension as a product of postcollisional melts.

The study area is part of the northern YB (fig. 2*a*). Metamorphic, ophiolitic mélange, and granitoid/syenitoid rocks represent the basement of the study area. Volcanosedimentary assemblages overlie these basement rocks (fig. 2*b*). The oldest lithologic unit in the study area is the metamorphic rocks, which, found in small exposures consisting of gneisses, schists, and marbles, also appear to correlate with metamorphites elsewhere in the CACC. Ophiolitic mélange rocks were exposed mostly in the southwestern part of the study area and include radiolarian cherts, pelagic limestone, and volcanic rocks. Granitoid/syenitoid rocks constitute plutonic rocks of the study area. These rocks comprise mainly granites, granodiorites, monzonites, and tonalites (Erler and Göncüoğlu 1996). The contacts between the granitoid/syenitoid rocks and the metamorphic and ophiolitic mélange rocks are mostly either covered or disrupted by young fault systems. However, in limited portions of the study area, the granitoid/syenitoid rocks contain enclaves of radiolarian cherts and pelagic limestone, indicating that they slightly predate the granitoids/syenitoids. Other units in the study area are the Eocene and Mio-Pliocene volcanosedimentary rocks. These rocks unconformably overlie all the rocks cited above. Locally, the contact between them is tectonic. The Eocene unit can be subdivided into two assemblages: (1) basal conglomerate, sandstone, interbedded bituminous shale, and coal seams of the lower assemblage and (2) fossil-bearing sandy limestone, tuffaceous deposits, and lava flows of the upper assemblage. The Mio-Pliocene unit overlies basement rocks and the Eocene units, comprising fluvial conglomerate, sandstone, and lacustrine mudstone.

The Kerkenez Granitoid and Ductile Shear Zones

The Kerkenez granitoid (KRG) is an intrusive body that has been separated from other bodies by cover units and/or faults in the YB. The northern and southern sides of the KRG have been overlain by Eocene and Mio-Pliocene units, respectively. The southwestern side of this body was bordered by rocks of ophiolitic mélange. The geological contact of both units is commonly disrupted by young faults and locally covered by Quaternary deposits. Within the limited area, intrusive relations between the KRG and the ophiolitic mélange are seen, suggesting that the KRG is posttectonic with respect to the ophiolitic rocks.

The KRG, composed primarily of hornblende quartz monzonite and hornblende granite, is cut by numerous mafic and felsic dikes. Hornblende quartz monzonite and hornblende granite are light to medium gray, medium/coarse grained, and equigranular to slightly porphyritic. They consist of feldspar (K-feldspar, plagioclase), quartz, and hornblende. Accessory minerals include titanite, apatite, zircon, allanite, and opaque minerals. These rocks are generally unaltered. Along the fault zones, however, hornblende is commonly chloritized, and feldspars experience significant alteration to sericite and kaolinite. Mafic and felsic dykes vary in thickness from a few centimeters to a few meters and trend both northeast and northwest. The black to dark green diorites make up the mafic dikes of the study area. They are texturally fine and/or medium/large grained and are cut by aplitic dikes. The diorites contain mainly hornblende, plagioclase, and local pyroxene, found in the core of the hornblende grains. Minor titanite, apatite, zircon, and opaque minerals are present. Felsic dikes include quartz-syenite porphyry, pegmatite, and aplite with granitic composition. Quartz-syenite porphyry contains a distinct flow structure accentuated by the alignment of pink K-feldspar crystals. It shows a profound northeast-southwest-trending mineral lineation defined by the aligned K-feldspar and plagioclase, indicating close relation to the magma intrusion and tectonics. A coarse-grained pegmatite, exposed in limited outcrops, is composed of feldspars and quartz with minor biotite. The aplite dikes are fine grained and resistant, consisting of quartz and feldspar with rare hornblende and biotite. Interestingly, within the KRG, numerous and variably thick northeast-southwest-trending tourmaline-breccia veins were formed with B-rich fluids of the magma. They range in thickness from 50 cm to 8 m and are mostly northeast trending. In the field, they display variable internal structural features, such as massive, stromatic, and breccia structures.

The study area contains local northeast-trending and northwest-dipping ductile shear zones characterized by discrete mylonitic shear zones. The zones are wide, from a few centimeters to several meters thick, and extend several hundred meters laterally. They are developed mostly within the KRG and can be traced discontinuously in the ophiolitic mélange exposed in the southwest of the study area (fig. 2*a*). They are commonly truncated by young faults. The zones in the KRG seem to have formed within hornblende quartz monzonite and are not seen cutting the dikes of the KRG. There is no sharp contact between the ductile shear zones and their protolith rocks of the KRG; instead, hornblende quartz monzonite grades to rocks of the shear zones. It is obvious that there are distinct

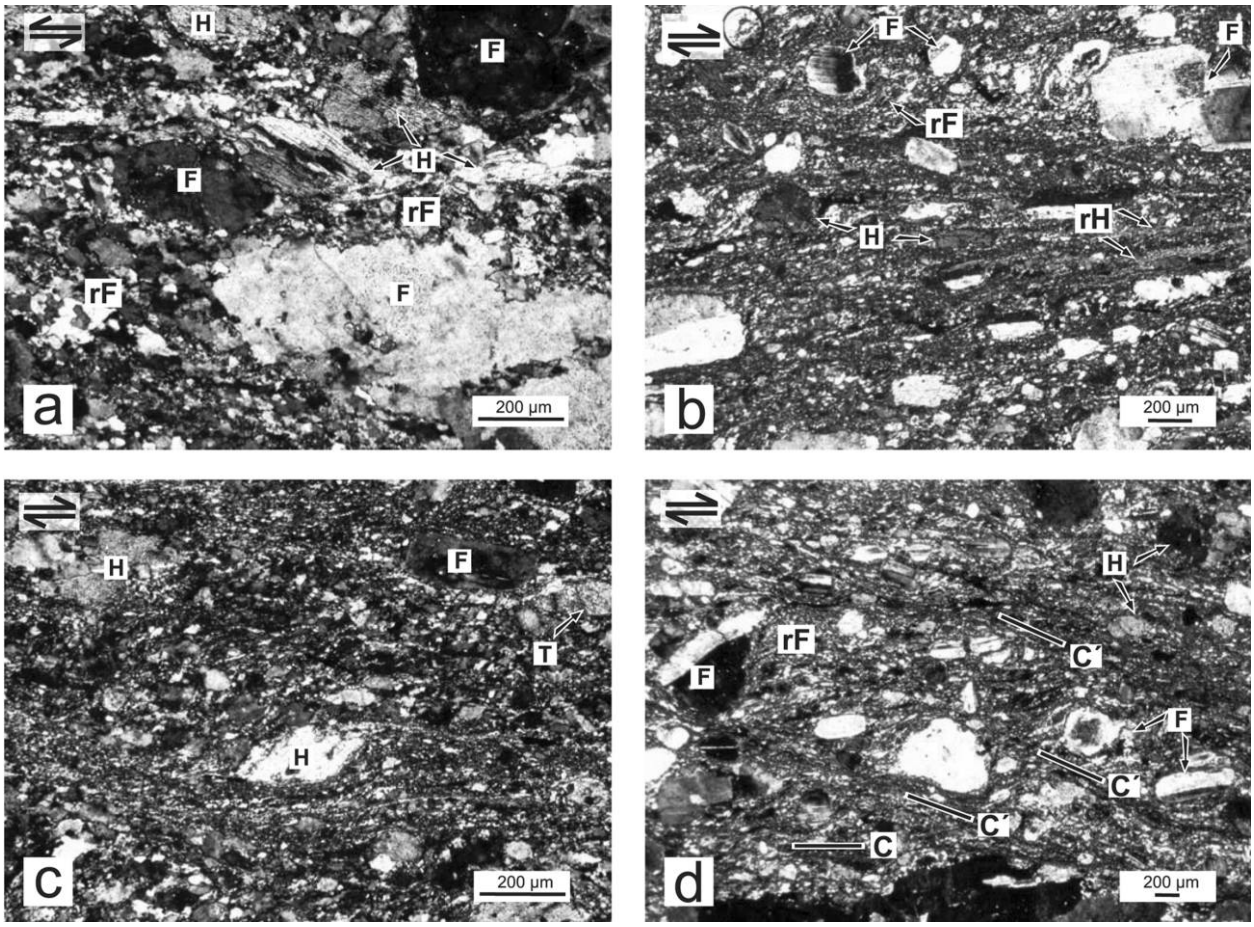

Figure 3. Photomicrographs from standard covered thin sections showing microstructural features of deformed grains in the extensional mylonitic shear zone (polarized light). *Scale bar* = 200 μm. *a*, Recrystallized feldspar and hornblende fragments. Relict feldspar is surrounded by recrystallized feldspar, indicating core-mantle structure. Note that relict feldspar porphyroclasts have irregular boundaries. Recrystallized feldspars show preferred orientations. *b*, Hornblende porphyroclast and recrystallized hornblende grains form mylonitic foliation. *c*, Microphotograph showing asymmetric hornblende and titanite porphyroclast indicating top-to-the-northwest shear sense. *d*, Photomicrograph showing detailed view of the relationship between C and C′ surfaces, suggesting top-to-the-northwest shear sense. *rF* = recrystallized feldspar; *H* = hornblende; *F* = feldspar; *rH* = recrystallized hornblende; *T* = titanite porphyroclast.

textural differences between rocks of the KRG and rocks of the shear zones. Ductile shear zones are characterized by mylonitic rocks with foliations and lineations. Mylonitic foliation, which is defined by fine-grained grains and elongate plagioclase and hornblende porphyroclasts, tends to strike mainly to the northeast. The foliation dips to the northwest at 08°–25° (fig. 2*c*, 2*d*). Intense mylonitic foliation is variable within the zones. More intense mylonitic foliation could be seen through the middle of the zones, indicating increasing amounts of strain. The mylonitic foliation contains variable down-dip stretching lineations, defined by elongated clasts of feldspar, quartz, and hornblende plus elongated mineral aggregates. Stretching lineations plunge gently to the northwest, with an average orientation of 12°–334° NW exposed in the KRG and 20°–314° NW exposed in the mélange rocks (fig. 2*c*, 2*d*).

In thin sections, the shear zone is commonly protomylonitic and mylonitic in character. The mylonites consist of porphyroclasts (feldspar, hornblende) of various sizes and a fine-grained matrix (fig. 3). The bulk of the matrix contains recrystallized quartz, feldspar, hornblende, and grain-sized feldspar and hornblende reduced by fracturing. Mylonitic foliation is defined by recrystallized quartz ribbons, elongated fine-grained tails composed of recrystallized feldspars and hornblende, and elon-

gated porphyroclasts of feldspar, hornblende, and titanite. Feldspar grains in the mylonites include undulose extinction, bending, subgrain formation, recrystallization, and fracturing, suggesting that the operative deformation mechanism is dislocation creep (cf. Tullis and Yund 1985, 1991; fig. 3*a*, 3*b*). Some feldspar porphyroclasts are surrounded by fine recrystallized grains, indicating core-and-mantle structure. Some feldspar porphyroclasts are cut by recrystallized feldspar and quartz-filled extension fractures, resulting in elongated feldspar grains along mylonitic foliation. Hornblende grains also display both brittle and ductile features. In samples, some hornblende porphyroclasts are disseminated, and fragments are strung out along mylonitic foliation (fig. 3*a*). The most common microstructure observed in hornblende is undulose extinction. A few hornblende porphyroclasts are cut by feldspar-filled extension fractures. Recrystallized hornblende grains form a banded structure representing mylonitic foliation (fig. 3*b*). Rarely, recrystallized hornblendes wrap around feldspar porphyroclasts. In samples, quartz microstructures included recrystallized grains. They form ribbons characterized by recrystallized grains with a strong grain-shape orientation. All of the above microstructural features of quartz, feldspar, and hornblende indicate that the shear zone in the KRG formed at temperatures of about 400°–500°C (cf. Simpson 1985; Passchier and Trouw 1996). This suggests that the mylonites in the study area formed under greenschist and lower amphibolite facies conditions.

Asymmetric porphyroclasts and composite shear bands are useful shear sense indicators in the shear zone within the KRG (cf. Passchier and Simpson 1986; Passchier and Trouw 1996; Snoke et al. 1998; Isik et al. 2003; fig. 3*c*, 3*d*). Porphyroclasts are composed of predominantly feldspar, hornblende, and lesser amounts of titanite and opaque minerals. They often have narrow mantles, variably sized elongated tails, and dynamically recrystallized feldspar, hornblende, and quartz, suggesting a sense of shear where the upper levels moved up to the northwest (fig. 3*c*).

Composite structures are characterized by S, C, and C′ surfaces and their angular relations in the shear zone. The S surfaces are defined by aligned feldspar grains, while the C surfaces (main mylonitic foliation) are defined by recrystallized quartz, feldspar, and hornblende and reoriented feldspar and hornblende. The C′ surfaces cut across the C surface and are defined by fine-grained feldspar, hornblende, and retort-shaped hornblende and feldspar grains plus porphyroclast tails that merge into the C surface (fig. 3*d*). As with asymmetric porphyroclasts, the angular relationships of the composite shear bands suggest a top-to-the-northwest shear sense.

As mentioned above, ductile shear zones within the KRG are characterized by a mylonitic foliation, accompanying down-dip stretching lineations and asymmetric kinematic indicators. A similar but weak foliation and lineation pattern is also found in shear zones exposed in the ophiolitic mélange. Within the shear zones, foliation strikes mainly northeast and is shallowly dipping. The stretching lineation plunges gently northwest. Equal-area projections do not disperse, suggesting that these lineations developed under the same tectonic regime. The sense of displacement of these zones has been determined from orientations of stretching lineations and kinematic indicators. Kinematic indicators in these zones display northwest-southeast-trending displacements. The character of these zones is questionable; they are either normal or folded reverse zones. In fact, it is difficult to show clear evidence about the character of these zones because they were developed mainly in the KRG and have limited exposures in the ophiolitic unit. In addition, the contact between the KRG and the ophiolitic unit was mainly obscured by young faults. The following findings and interpretations give clues to the extensional character of these zones. (1) The zones include kinematic indicators showing that the northwest blocks are downthrown relative to the southeast blocks. (2) These ductile shear zones have mylonitic foliations that are northwest dipping. In the case of reverse or folded reverse, some zones with opposite dip directions should be present. (3) Numerous northeast-southwest-trending tourmaline veins within the KRG suggest that the KRG underwent significant northwest-southeast-trending extension. The age of the tourmaline veins is pre-Eocene because pebbles of tourmaline are found in the Eocene units. (4) Our field observations in the region reveal some thrust faults that displace the granitoid onto the Eocene and/or Mio-Pliocene units with a top-to-the-south sense of shear. These faults have been interpreted as structures younger than the ductile shear zones because they overprint the ductile shear zones and show an opposite shear sense.

On the basis of field observations and microscopic studies, combined with regional geological information, we interpreted the ductile shear zones described above as developed by extensional tectonism. Similarly, an extensional ductile shear zone, called the Emizözü shear zone, has been docu-

mented in the Ağaçören granitoid within the western part of the CACC (Isik 2008).

$^{40}Ar/^{39}Ar$ Geochronology

Sample Selection and Descriptions. Samples were collected in the KRG of the YB for $^{40}Ar/^{39}Ar$ dating at locations indicated in figure 2*b*. Two samples (03V-34 and 03V-56) were chosen from granitoid that shows no signs of ductile or brittle deformation. Two mylonitized samples (03V-47 and 03V-51) from the ductile shear zone were chosen at locations where the granitoid displays mylonitic foliation and stretching lineations.

Sample 03V-34 is hornblende granite, and it was located in the western part of the KRG. It is light gray in color and equigranular in texture. Plagioclase occurs as subhedral minerals and commonly displays twinning. K-feldspar is subhedral and encloses plagioclase and hornblende minerals. Some K-feldspar is slightly altered to clay minerals. Quartz minerals are anhedral. Hornblende occurs as euhedral crystals but is mostly subhedral.

Samples 03V-47 and 03V-51 were obtained from ductilely deformed quartz monzonite within the shear zone. Sample 03V-51 was collected only a few tens of meters from sample 03V-47. Both samples have a similar structure and display mylonitic textures in hand-specimen and thin-section forms. The samples have typical ductile structures, such as mylonitic foliation and stretching lineations. The mylonitic structure is defined by elongated feldspars, hornblendes, and quartz minerals; individual minerals have preferred orientations and display brittle and/or ductile deformational structures.

The sample 03V-56 is hornblende quartz monzonite that is the protolith of the mylonitic rocks (samples 03V-47 and 03V-51). The sample is gray, medium grained, and equigranular but slightly porphyritic. Plagioclase occurs as subhedral minerals. K-feldspar is subhedral and contains fine-grained plagioclase and hornblende minerals as inclusions. Intergrowths of quartz and feldspar grains (myrmekitic and micrographic textures) are observed along the contact of the plagioclase and K-feldspar minerals. Hornblende is medium grained and subhedral. Quartz forms 10% of the rock composition.

Method. The samples were wrapped in aluminum foil packets; stacked in an aluminum canister with three aliquots (~6 mg) of the irradiation standard LP-6 biotite (Odin et al. 1982), with a calibrated $^{40}Ar/^{39}Ar$ age of 128.4 ± 0.2 Ma based on Fish Canyon sanidine (28.02 ± 0.28 Ma; Baksi et al. 1996; Renne et al. 1998); and irradiated in the VT-C position of the Tsing Hua open-pool reactor for 30 h. The *J* values were calculated from the gas compositions of total fusions of the irradiation standards by using a double-vacuum Mo furnace. The neutron flux gradient across the top and bottom of the irradiation canisters was less than 0.9%, as indicated by the variation of *J* values from the flux monitors.

After irradiation, the samples were loaded into an Al sample holder and heated with a NdYAG laser operated in continuous mode. Step heating was achieved with increasing energy of the laser power. The released gas was purified with two Zr-Al getters and analyzed with a VG3600 mass spectrometer at National Taiwan University. Measured isotopic ratios were corrected for the effects of mass discrimination, system blanks, radioactive decays, and isotope interferences produced during irradiation by employing factors reported by Lo et al. (2002) for the reactor used in this study.

Apparent $^{40}Ar/^{39}Ar$ ages were calculated from the corrected isotopic ratios by using the decay constants and isotopic abundance ratios given by Steiger and Jager (1977). The 1 SD intralaboratory uncertainties in each apparent age are reported. The analytical data are presented in table A1 (available in the online edition or from the *Journal of Geology* office) and are plotted as age spectra and $^{36}Ar/^{40}Ar$–$^{39}Ar/^{40}Ar$ isotope correlation diagrams in figures 4 and 5 for each sample. Table 2 summarizes the results. Total gas ages were computed from the sum total of the peak heights, and their errors were calculated from the square root of the sum square of the peak-height errors for all steps. Plateau ages were calculated with the same approach but using only those contiguous steps yielding dates that met the criteria discussed by Baksi (2006). In the $^{36}Ar/^{40}Ar$–$^{39}Ar/^{40}Ar$ correlation diagrams, the cubic least squares fitting scheme outlined by York (1969) was employed to regress the data. The regression line yielded two intercepts; the inverse of the $^{39}Ar/^{40}Ar$ intercept produced a so-called intercepted date, whereas the inverse of the $^{36}Ar/^{40}Ar$ intercept indicated the composition of a nonradiogenic argon component.

Results. As shown in figures 4 and 5, most of the samples show fairly flat profiles for the age spectra, with some disturbances in the low- and high-temperature steps in some of the samples (03V-34 hornblende and K-feldspar, 03V-56 hornblende, and 03V-47 K-feldspar). Without further clarification, these disturbances may have been due to the outgassing of minor impurities (alteration phases) in mineral grains, which are apparent under the microscope. Certainly, argon diffusion

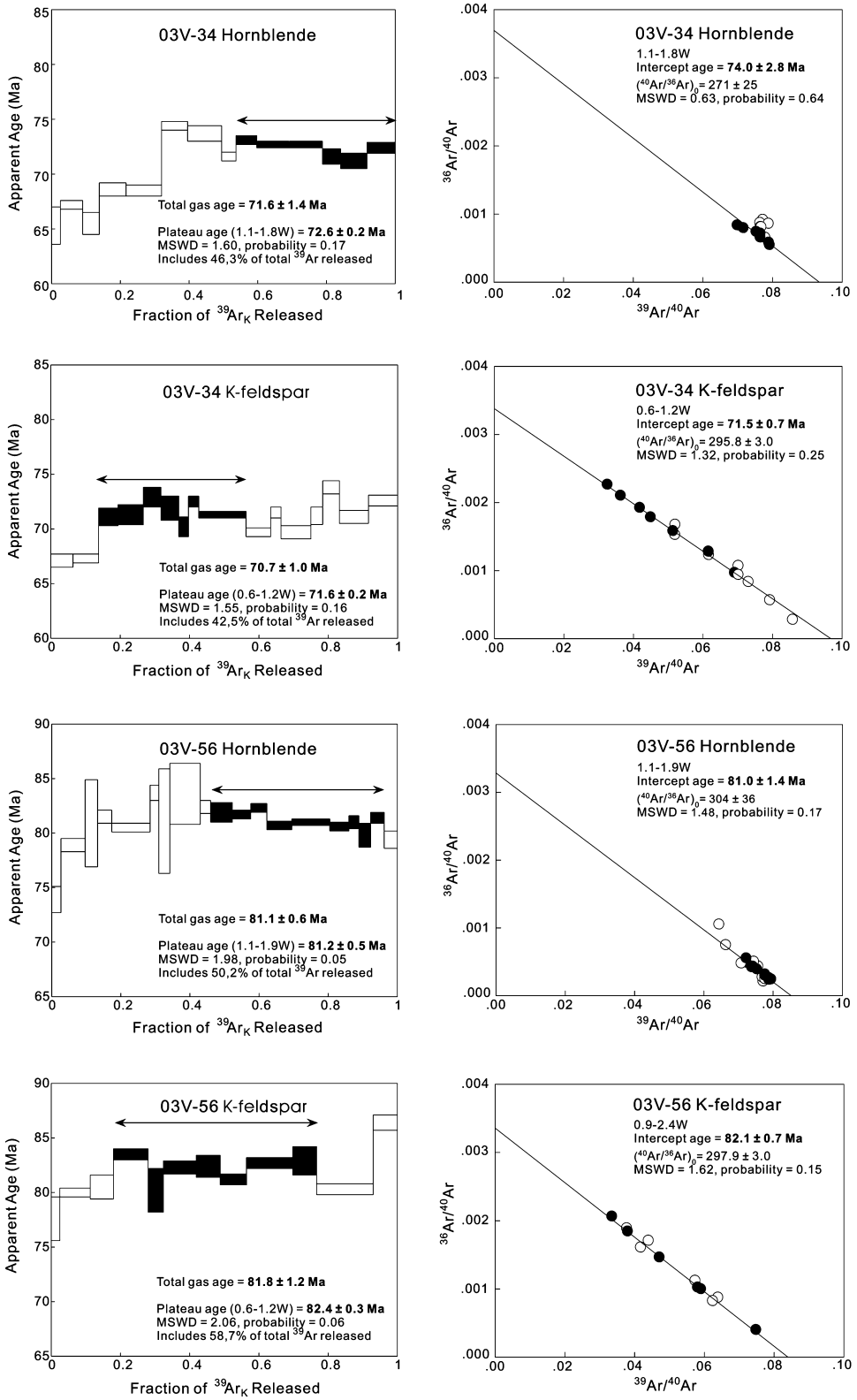

Figure 4. The $^{40}Ar/^{39}Ar$ age spectra and isotope correlation diagrams for samples from the Kerkenez granitoid. *Top row,* sample 03V-34 hornblende; *second row,* sample 03V-34 K-feldspar; *third row,* sample 03V-56 hornblende; *bottom row,* sample 03V-56 K-feldspar.

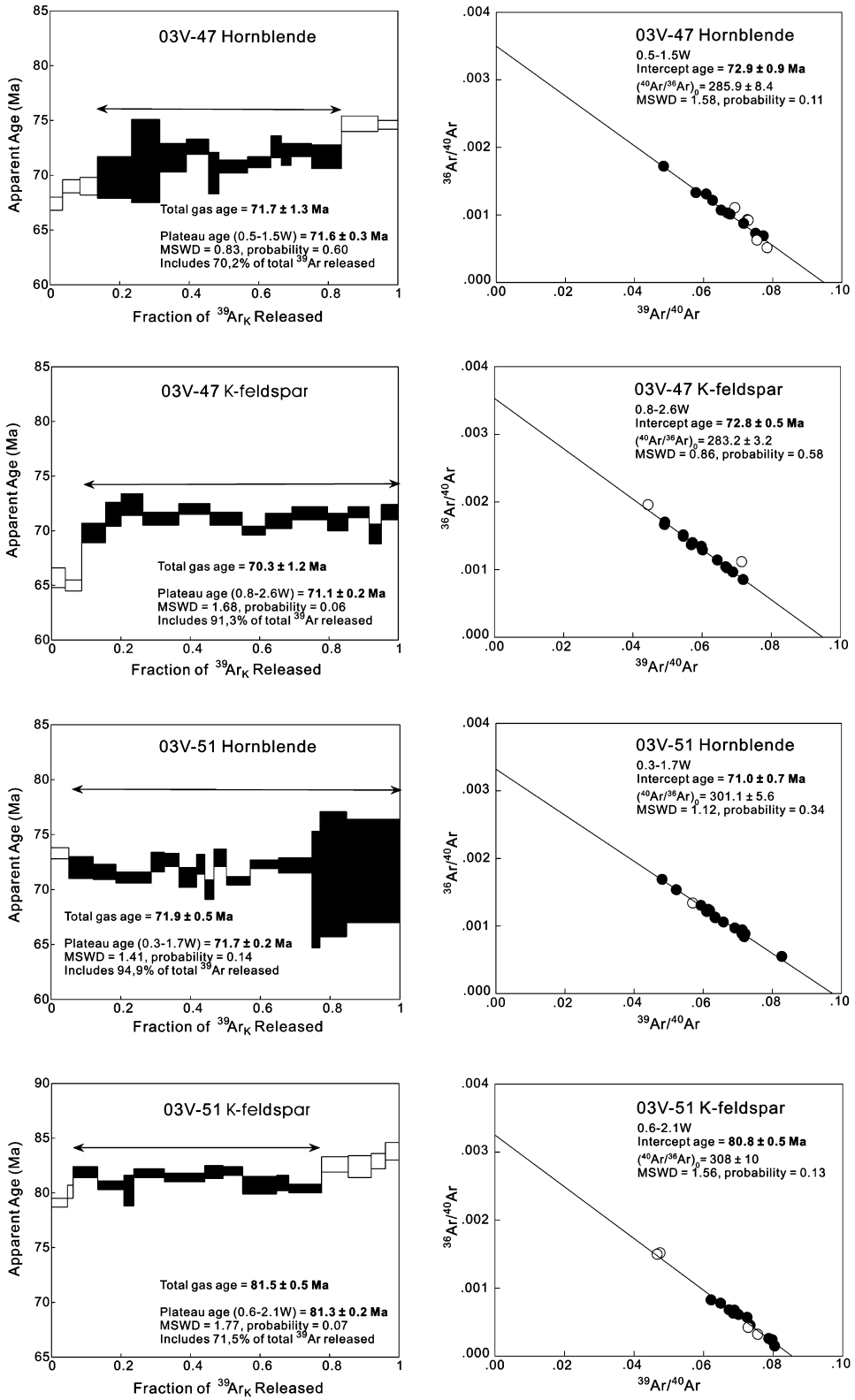

Figure 5. The $^{40}Ar/^{39}Ar$ age spectra and isotope correlation diagrams for samples from ductile shear zone in the Kerkenez granitoid. *Top row*, sample 03V-47 hornblende; *second row*, sample 03V-47 K-feldspar; *third row*, sample 03V-51 hornblende; *bottom row*, sample 03V-51 K-feldspar.

Table 2. Summary of $^{40}Ar/^{39}Ar$ Dating Results

Sample and mineral	Total gas age ± 1σ (Ma)	Plateau plot						Isotope correction plot			
		Step[a]	N[b]	^{39}Ar (% of total)	Plateau age (Ma) ± 1σ	$MSWD_{(n-1)}$	P[c]	Intercept age ± 1σ (Ma)	$(^{40}Ar/^{36}Ar)_0$ ± 1σ	$MSWD_{(n-2)}$	P[c]
03V-34:											
Hornblende	71.6 ± 1.4	1.1–1.8	6	46.3	72.6 ± .2	1.60	.17	74.0 ± 2.8	271 ± 25	.63	.64
K-feldspar	70.7 ± 1.0	.6–1.2	7	42.5	71.6 ± .2	1.55	.16	71.5 ± .7	295.8 ± 3.0	1.32	.25
03V-47:											
Hornblende	71.7 ± 1.3	.5–1.5	11	70.2	71.6 ± .3	.83	.60	72.9 ± .9	285.9 ± 8.4	1.58	.11
K-feldspar	70.3 ± 1.2	.8–2.6	13	91.3	71.1 ± .2	1.68	.06	72.8 ± .5	283.2 ± 3.2	.86	.58
03V-51:											
Hornblende	71.9 ± .5	.3–1.7	15	94.9	71.7 ± .2	1.41	.14	71.0 ± .7	301.1 ± 5.6	1.12	.34
K-feldspar	81.5 ± .5	.6–2.1	10	71.5	81.3 ± .2	1.77	.07	80.8 ± .5	308 ± 10	1.56	.13
03V-56:											
Hornblende	81.1 ± .6	1.1–1.9	9	50.2	81.2 ± .5	1.98	.05	81.0 ± 1.4	304 ± 36	1.48	.17
K-feldspar	81.8 ± 1.2	.9–2.4	7	58.7	82.4 ± .3	2.06	.06	82.1 ± .7	297.9 ± 3.0	1.62	.15

[a] Laser energy of plateau steps (in W).
[b] Number of plateau steps.
[c] Probability at 95% confidence level.

loss from mineral grains during thermal disturbance may also be responsible for the age depression in the low-temperature steps on the age spectrum. Excluding these disturbed steps, age spectrum plots for most samples evidently suggest meaningful plateaus over 50% of $^{39}Ar_K$ released for most samples (tables 2, A1) with meaningful mean square weighted deviate (MSWD) and *P* (probability) values (≥0.05), except for 03V-34 hornblende and K-feldspar. Data regression for gas compositions from the plateau steps yields $^{40}Ar/^{39}Ar$ initial values (285–308) not much different from that for atmospheric composition (295.5), with statistically meaningful MSWD values (0.85–1.62). The intercept ages (71.0 ± 0.7–82.1 ± 0.7 Ma) are all in agreement with their respective plateau ages (71.6 ± 0.3–82.4 ± 0.3 Ma; figs. 4, 5). These suggest that the argon isotopic systematics in most samples consist of mainly radiogenic and atmospheric components and that excess argon is not apparent. The obtained plateau ages for most samples, except 03V-34 hornblende and K-feldspar, should be geologically meaningful.

The age spectra for 03V-34 hornblende and K-feldspar appear to be very flat at high-temperature steps (fig. 4), but they fail to meet the plateau criteria proposed by Baksi (2006) because their compositions constitute only 46.3% and 42.5%, respectively, of the total ^{39}Ar released. The gas compositions of these microplateaus display consistent ages that agree well with each other within the 95% confidence level, and they lead to reasonable MSWD and *P* values (>0.5), yielding plateau ages of 72.6 ± 0.2 Ma for 03V-34 hornblende and 71.6 ± 0.2 Ma for 03V-34 K-feldspar (fig. 4). Moreover, the isotope correlation plots for these gas compositions also yield reasonable $^{40}Ar/^{39}Ar$ initial values (271 ± 25 and 295.8 ± 3.0) and intercept ages (74.0 ± 2.8 and 71.5 ± 0.7 Ma) consistent with their respective plateau ages (fig. 4; table 2). This would suggest that these microplateau ages for 03V-34 hornblende and K-feldspar may still be geologically meaningful even though disturbances of the isotopic systematics are apparent in these two samples.

Discussion

During Late Cretaceous time, the CACC experienced significant compression, as did many regions within the Alpine orogeny (e.g., Channell 1986; Dewey et al. 1989; Stampfli et al. 1998; Jolivet and Faccenna 2000; Rosenbaum et al. 2002). The northern CACC was the site of compressional deformation during this time. This deformation was characterized by the collision of the Anatolide-Tauride platform into the Pontides, obduction of ophiolite slabs, regional metamorphism, and significant amount of magma generation. Tectonic burial of pre-Cenozoic rocks to depths in the region was followed by emplacement of granitoids, uplift, and cooling. The intrusion of the KRG postdates early penetrative regional metamorphism and ophiolite obduction.

Cooling of the KRG. Considering the high closure temperatures (~500°C for hornblende and ~350°C for K-feldspar), hornblende and K-feldspar $^{40}Ar/^{39}Ar$ ages would provide an estimate of not only cooling age but also cooling rate when the closure temperatures are taken into consideration (McDougall and Harrison 1988). As in figure 4, K-feldspar $^{40}Ar/^{39}Ar$ plateau ages are very close to coexisting hornblende plateau ages in both 03V-56 hornblende quartz monzonite and 03V-34 hornblende granite. This would suggest that both hornblende quartz monzonite and hornblende granite in the KRG may have cooled rapidly, probably at a rate greater than 110°C/Ma, after emplacement. Considering such a rapid cooling rate, it may be further suggested that hornblende quartz monzonite may have been emplaced at around 81.2 ± 0.5 Ma, which appears to be slightly older than hornblende granite in the KRG, as indicated by the microplateau age for 03V-34 hornblende (72.6 ± 0.2 Ma; fig. 4). In the field, there is no outcrop evidence indicating the spatial relationship between the pattern of hornblende quartz monzonite and that of hornblende granite. However, the time constraints suggest that the emplacement and cooling of hornblende quartz monzonite took place slightly later than those for of hornblende granite. Additionally, on the basis of intrusive relations and $^{40}Ar/^{39}Ar$ ages, an upper age limit (~81 Ma) of the regional metamorphism in the metamorphites in the northern part of the CACC could be constrained. This interpretation can also be correlated to the isotopic age of metamorphic rocks (~84 Ma) in the southern part of the CACC reported by Whitney and Hamilton (2004).

Cooling of Ductile Shear Zone in the KRG. The KRG contains anastomosing mylonitic shear zones that display top-to-the-northwest shear senses. Deformed minerals, such as feldspar, display dynamic recrystallization, which indicates that formation of the ductile deformation in the zone occurred at a temperature of about 500°C. The timings of the ductile shear zone and related deformation in the KRG are clearly constrained with this study because deformation occurred at temperatures well above the temperature of argon retention, representing the cooling ages. Hornblende from samples

03V-47 and 03V-51 yields plateau ages of 71.6 ± 0.3 and 71.7 ± 0.2 Ma, respectively (fig. 5). These are interpreted to closely date cooling through temperatures required for retention of argon in hornblende (500°C; Harrison 1981). K-feldspar from sample 03V-47 yields a plateau age of 71.1 ± 0.2 Ma, but an age of 81.3 ± 0.2 Ma was obtained from K-feldspar from sample 03V-51 (fig. 5). It is clear that the deformed K-feldspar from sample 03V-47 records a younger age, consistent with the age of hornblende. We therefore adopt 71.6 ± 0.3 and 71.7 ± 0.2 Ma as the cooling ages of hornblende and K-feldspar, respectively, in the ductile shear zone. On the other hand, an age of 81.3 ± 0.2 Ma of the deformed K-feldspar does not seem to reflect the age of ductile deformation affecting the KRG (fig. 5). It is interesting to note that this age of K-feldspar appears to be consistent with that of K-feldspar from sample 03V-56, collected from the undeformed hornblende quartz monzonite that is the protolith of samples 03V-47 and 03V-51 (fig. 4). It is possible that the K-feldspar age of 81.3 ± 0.2 Ma may be inherited from the undeformed hornblende quartz monzonite.

We infer from field study and isotopic data in the study area that intrusive activity and ductile deformation in the KRG appear to have occurred in four steps. First, the intrusive activity defined by hornblende quartz monzonite occurred at 81 Ma. The second intrusive activity seems to be defined by hornblende granite. It yields an age of approximately 73 Ma, which suggests that there was a small time gap between two intrusive activities in the region. The outcrop patterns show that ductile deformation turned hornblende quartz monzonite into mylonites along the shear zones. The $^{40}Ar/^{39}Ar$ age data indicate that the age of the ductile shear zones in the region is between 72 and 71 Ma, suggesting that the shear zones began to form soon after the emplacement and cooling of hornblende granite. The other igneous activity in the region is represented by intrusion of mafic and felsic rocks.

Tectonic Implications. Erosion and tectonic denudation rates in central Turkey have not been well documented by previous authors. However, the new data, even if limited, shed light on the timing of metamorphism, granitoid intrusion, and ductile shearing of the granitoid related to the tectonic denudation in the northern part of the CACC. Regionally, the granitoids cut the metamorphites, which are widely exposed in central Turkey. The age of their peak metamorphism is about 85 Ma (Whitney and Hamilton 2004), which provides a lower age constraint for granitic magmatism.

In the northern part of the CACC, the KRG ranges in composition from quartz monzonite to syenite. The notable structures in the KRG are anastomosing discrete mylonite zones with top-to-the-northwest shear senses. The KRG and these shear zones are temporally linked. The microstructural features of deformed minerals in the shear zones suggest that the mylonites were formed at a relatively high temperature. Furthermore, some kinematic features of these zones suggest extensional deformation; extensional faulting and the generation of normal-sense brittle shear fractures plus tourmaline veins in the region also support this conclusion. On the basis of field observations, microstructural studies, and the available $^{40}Ar/^{39}Ar$ age data, we interpret the tectonic evolution of the KRG as follows.

During the Late Cretaceous, after the region was buried and metamorphosed in response to the closure of the IAE Ocean, the KRG intruded. At first, hornblende quartz monzonite was emplaced into relatively cooler host rock, such as the metamorphites and the ophiolitic unit. The cooling time of hornblende quartz monzonite is ~81 Ma. Shortly after, hornblende granite was emplaced and began to cool. The cooling of hornblende granite is constrained to between 72 and 73 Ma. This implies that hornblende quartz monzonite existed at relatively the same level of crust until about 72 Ma. After this time, the character of the deformation probably changed and the KRG was transported by the shear zones to a shallower crustal level. The $^{40}Ar/^{39}Ar$ of hornblendes from these zones indicates that the closure temperature for argon in the zone is about 71 Ma. This cooling event is interpreted to be associated with the beginning of extension in the region. Furthermore, these data imply that the metamorphism, emplacement, and cooling of the intrusives and ductile shearing of the intrusions were coeval and occurred in Late Cretaceous time.

Conclusions

The following main conclusions can be drawn from field, microscopic, and geochronologic studies of the northern part of the CACC.

1. The $^{40}Ar/^{39}Ar$ hornblende ages from hornblende quartz monzonite and hornblende granite indicate that the KRG began to be emplaced before ~81 Ma and cooled below the temperature of 500°C mainly between 81 and 72 Ma. The $^{40}Ar/^{39}Ar$ K-feldspar ages that are interpreted as the cooling ages of these rocks are slightly younger than the hornblende ages, implying relatively rapid exhumation.

2. The KRG contains discrete mylonitic extensional shear zones with kinematic indicators (e.g., asymmetric porphyroclasts and composite shear bands) displaying top-to-the-northwest shear senses. Microstructural features of deformed grains in the shear zone indicate greenschist and lower amphibolite facies-grade metamorphic conditions. The $^{40}Ar/^{39}Ar$ hornblende ages from mylonitic hornblende quartz monzonite from this zone indicate cooling through 500°C at 71 Ma. This isotopic age implies the timing of the onset of the extension regime in the region consistent with basin deposits of Late Maastrichtian age.

ACKNOWLEDGMENTS

Field study for this research was supported by the Scientific and Technical Research Council of Turkey (grant 103Y123). We thank F. Jourdan and an anonymous reviewer for their helpful and constructive criticism. We also thank A. Anderson for his fastidious editorial handling.

REFERENCES CITED

Akıman, O.; Erler, A.; Göncüoğlu, M. C.; Güleç, N.; Geven, A.; Türeli, K.; and Kadıoğlu, Y. 1993. Geochemical characteristics of granitoids along the western margin of the central Anatolian crystalline complex and their tectonic implications. Geol. J. 28: 371–382.

Ataman, G. 1972. The preliminary study on the radiometric age of Cefalik Dağı that is one of the granitic-granidioritic bodies in the SW of Ankara. Hacettepe Univ. Yerbilimleri Dergisi 2:44–49 (in Turkish).

Ayan, M. 1963. Contribution a l'étude pétrographique et géologique de la region située au Nord-Est de Kaman. Bull. Miner. Res. Explor. Inst. Turk. 115:13–32.

Aydın, N. S.; Göncüğlu, M. C.; and Erler, A. 1998. Latest Cretaceous magmatism in the central Anatolian crystalline complex: review of field, petrographic and geochemical features. Turk. J. Earth Sci. 7:259–268.

Baksi, A. K. 2006. Guidelines for assessing the reliability of $^{40}Ar/^{39}Ar$ plateau ages: application to ages relevant to hotspot tracks. http://www.mantleplumes.org/ArAr.html.

Baksi, A. K.; Archibald, D. A.; and Farrar, E. 1996. Intercalibration of $^{40}Ar/^{39}Ar$ dating standards. Chem. Geol. 129:307–324.

Bingen, B.; Boven, A.; Punzalan, L.; Wijbrans, J. R.; and Demaiffe, D. 1998. Hornblende $^{40}Ar/^{39}Ar$ geochronology across terrane boundaries in the Sveconorwegian Province of South Norway. Precambrian Res. 90: 159–185.

Boztuğ, D. 1995. Petrography, major element geochemistry and petrogenesis of the eastern part of the Yozgat batholith from the Kırşehir block, south of Sorgun town, central Anatolia, Turkey. Istanbul Univ. Yerbilimleri Dergisi 9:1–20 (in Turkish).

———. 1998. Post-collisional central Anatolian alkaline plutonism, Turkey. Turk. J. Earth Sci. 7:145–165.

———. 2000. S-I-A intrusive associations: geodynamic significance of synchronism between metamorphism and magmatism in central Anatolia, Turkey. *In* Bozkurt, E.; Winchester, J. A.; and Piper, J. A. D., eds. Tectonics and magmatism in Turkey and the surrounding area. Geol. Soc. Lond. Spec. Publ. 173:441–458.

Boztuğ, D.; Otlu, N.; and Tatar, S. 2004. Geological and petrological remarks revealing the differential tectonic uplift in the exhumation history of the collision-related central Anatolian intrusives, Turkey. *In* Fifth International Symposium on Eastern Mediterranean Geology, Proc., Thessalonica, p. 45–48.

Channel, J. E. T. 1986. Palaeomagnetism and continental collision in the Alpine Belt and the formation of late-tectonic extensional basins palaeogeography of Adria. *In* Coward, M. P., and Ries, A. C., eds. Collision tectonics. Geol. Soc. Lond. Spec. Publ. 19:261–284.

Clark, M., and Robertson, A. H. F. 2005. Uppermost Cretaceous–Lower Tertiary Ulukışla Basin, south-central Turkey: sedimentary evolution of part of a unified basin complex within an evolving Neo-Tethyan suture zone. Sediment. Geol. 173:15–51.

Dewey, J. F.; Helman, M. L.; Turco, E.; Hutton, D. H. W.; and Knott, S. D. 1989. Kinematics of the western Mediterranean. *In* Coward, M. P.; Dietrich, D.; and Park, R. G., eds. Alpine tectonics. Geol. Soc. Lond. Spec. Publ. 23:265–283.

Dirik, K.; Göncüoğlu, M. C.; and Kozlu, H. 1999. Stratigraphy and pre-Miocene tectonic evolution of the southwestern part of the Sivas Basin. Geol. J. 34: 303–319.

Erdoğan, B.; Akay, E.; and Uğur, S. M. 1996. Geology of the Yozgat region and evolution of the collisional Çankırı Basin. Int. Geol. Rev. 38:788–806.

Erler, A., and Göncüoğlu, M. C. 1996. Geologic and tectonic setting of the Yozgat batholith, northern central Anatolian crystalline complex, Turkey. Int. Geol. Rev. 38:714–726.

Fayon, A. K.; Whitney, D. L.; Teyssier, C.; Garver, J. I.; and Dilek, Y. 2001. Effects of plate convergence obliquity on timing and mechanisms of exhumation of a mid-crustal terrain, the central Anatolian crystalline complex. Earth Planet. Sci. Lett. 192:191–205.

Fossen, H., and Dunlap, W. J. 1998. Timing and kinematics of Caledonian thrusting and extensional collapse,

southern Norway: evidence from $^{40}Ar/^{39}Ar$ thermochronology. J. Struct. Geol. 20:765–781.

Foster, D. A.; Miller, C. E.; Harrison, T. M.; and Hoisch, T. D. 1992. $^{40}Ar/^{39}Ar$ thermochronlogy and thermobarometry of metamorphism, plutonism, and tectonic denudation in the Old Woman Mountains area, California. Geol. Soc. Am. Bull. 104:176–191.

Göncüoğlu, M. C. 1986. Geochronologic data from the southern part (Niğde area) of the central Anatolian massif. Bull. Miner. Res. Explor. Inst. Turk. 105/106: 83–96.

Göncüoğlu, M. C.; Köksal, S.; and Floyd, P. A. 1997. Post-collisional A-type magmatism in the central Anatolian crystalline complex: petrology of the Idis Dagi intrusives (Avanos, Turkey). Turk. J. Earth Sci. 6:65–76.

Göncüoğlu, M. C.; Toprak, V.; Kusçu, I.; Erler, A.; and Olgun, E. 1991. Geology of the western part of the central Anatolian massif. Turkish Petroleum Corporation Report 2909. Ankara, Turkish Petroleum Corporation (in Turkish).

Görür, N.; Oktay, F. Y.; Seyman, İ.; and Şengör, A. M. C. 1984. Paleotectonic evolution of the Tuzgölü Basin Complex, central Turkey: sedimentary record of a Neo-Tethyan closure. *In* Dixon, J. E., and Robertson, A. H. F., eds. The geological evolution of the eastern Mediterranean. Geol. Soc. Lond. Spec. Publ. 17:467–482.

Görür, N.; Tüysüz, O.; and Şengör, A. M. C. 1998. Tectonic evolution of the central Anatolian basins. Geol. Soc. Int. Geol. Rev. 40:831–850.

Güleç, N. 1994. Rb-Sr isotope data from the Agaçören granitoid (east of Tuz Gölü): geochronology and genetical implications. Turk. J. Earth Sci. 3:39–43.

Gürer, Ö. F., and Aldanmaz, E. 2002. Origin of the Upper Cretaceous–Tertiary sedimentary basins within the Tauride-Anatolide platform in Turkey. Geol. Mag. 139:191–197.

Harrison, T. M. 1981. Diffusion of ^{40}Ar in hornblende. Contrib. Mineral. Petrol. 78:324–331.

Harrison, T. M.; Lovera, O. M.; and Heizler, M. T. 1991. $^{40}Ar/^{39}Ar$ results for alkali feldspars containing diffusion domains with differing activation-energy. Geochim. Cosmochim. Acta 55:1435–1448.

İlbeyli, N.; Pearce, J. A.; Thirlwall, M. F.; and Mitchell, J. G. 2004. Petrogenesis of collision-related plutonics in central Anatolia, Turkey. Lithos 72:163–182.

Isik, V. 2008. Ductile shear zone in granitoid of the central Anatolian crystalline complex, Turkey: implications for initiation of the Tuzgölü Basin during the Late Cretaceous extensional deformation. J. Asian Earth Sci. 34, forthcoming.

Isik, V.; Seyitoglu, G.; and Çemen, I. 2003. Ductile-brittle transition along the Alasehir shear zone and its structural relationship with the Simav detachment, Menderes massif, western Turkey. Tectonophysics 374: 1–18.

Isik, V.; Tekeli, O.; and Seyitoğlu, G. 2004. The $^{40}Ar/^{39}Ar$ age of extensional ductile deformation and granitoid intrusions in the northern Menderes core complex: implications for the initiation of extensional tectonics in western Turkey. J. Asian Earth Sci. 23:555–566.

Jolivet, L., and Faccenna, C. 2000. Mediterranean extension and the Africa-Eurasia collision. Tectonics 19: 1095–1106.

Jourdan, F.; Féraud, G.; Bertrand, H.; Kampunzu, A. B.; Tshoso, G.; Le Gall, B.; Tiercelin, J. J.; and Capiez, P. 2004. The Karoo triple junction questioned: evidence from $^{40}Ar/^{39}Ar$ Jurassic and Proterozoic ages and geochemistry of the Okavango dyke swarm (Botswana). Earth Planet. Sci. Lett. 222:989–1006.

Kadıoğlu, Y. K.; Dilek, Y.; Güleç, N.; and Foland, K. A.. 2003. Tectonomagmatic evolution of bimodal plutons in the central Anatolian crystalline complex, Turkey. J. Geol. 111:671–690.

Ketin, İ. 1955. Yozgat bölgesinin jeolojisi ve Orta Anadolu masifinin tektonik durumu. Turk. Jeol. Bul. 6:1–40 (in Turkish).

Kohn, B. P.; Feinstein, S.; Foster, D. A.; Steckler, M. S.; and Eyal, M. 1997. Thermal history of the eastern Gulf of Suez. II. Reconstruction from apatite fission track and $^{40}Ar/^{39}Ar$ K-feldspar measurements. Tectonophysics 283:219–239.

Köksal, S.; Romer, R. L.; Göncüoğlu, M. C.; and Toksoy-Köksal, F. 2004. Timing of post-collisional H-type to A-type granitic magmatism: U-Pb titanite ages from the Alpine central Anatolian granitoids (Turkey). Int. J. Earth Sci. 93:974–989.

Kuruç, A. 1990. Rb-Sr geochemistry of syenitoids from Kaman-Kırşehir region. MS thesis, Hacettepe University, Ankara (in Turkish).

Lips, A. L. W.; White, S. H.; and Wijbrans, J. R. 1998. $^{40}Ar/^{39}Ar$ laserprobe direct dating of discrete deformational events: a continuous record of early Alpine tectonics in the Pelagonian Zone, NW Aegean area, Greece. Tectonophysics 298:133–153.

Lo, C.-H.; Chung, S.-L.; Lee, T.-Y.; and Wu, G.-Y. 2002. Age of the Emeishan flood magmatism and relations to Permian-Triassic boundary events. Earth Planet. Sci. Lett. 198:449–458.

McDougall, I., and Harrison, T. M. 1988. Geochronology and thermochronology by the $^{40}Ar/^{39}Ar$ method. New York, Oxford University Press.

Odin, G. S.; Adams, C. J.; Armstrong, R. L.; Bagdasaryan, G. P.; Baksi, A. K.; Balogh, K.; Barnes, I. L.; et al. 1982. Interlaboratory standards for dating purposes. *In* Odin, G. S., ed. Numerical dating in stratigraphy. Chichester, Wiley, p. 123–149.

Okay, A. I., and Tüysüz, O. 1999. Tethyan sutures of northern Turkey. *In* Durand, B.; Jolivet, L.; Horvath, F.; and Sreanne, M., eds. The Mediterranean basins: Tertiary extension within the Alpine orogen. Geol. Soc. Lond. Spec. Publ. 156:475–515.

Passchier, C. W., and Simpson, C. 1986. Porphroclast systems as kinematic indicators. J. Struct. Geol. 8: 831–844.

Passchier, C. W., and Trouw, R. A. J. 1996. Micro-tectonics. Berlin, Springer, 289 p.

Poisson, A. 1986. The Anatolian micro-continent in the

eastern Mediterranean context: the Neo-Tethian troughs. Sci. Terre Mem. 47:311–328.

Poisson, A.; Guezou, J. C.; Öztürk, A.; Inan, S.; Temiz, H.; Gürsoy, H.; Kavak, K. S.; and Özden, S. 1996. Tectonic setting and evolution of the Sivas Basin. Int. Geol. Rev. 38:833–853.

Reddy, S. M.; Potts, G. J.; and Kelley, S. P. 2001. $^{40}Ar/^{39}Ar$ ages in deformed potassium feldspar: evidence of microstructural control on argon systematics. Contrib. Mineral. Petrol. 141:186–200.

Renne, P. R.; Swisher, C. C.; Deino, A. L.; Karner, D. B.; Owens, T. L.; and DePaolo, D. J. 1998. Intercalibration of standards, absolute ages and uncertainties in $^{40}Ar/^{39}Ar$ dating. Chem. Geol. 145:117–152.

Robertson, A. H. F., and Dixon, J. E. 1984. Introduction: aspects of the geological evolution of the eastern Mediterranean. *In* Dixon, J. E., and Robertson, A. H. F., eds. The geological evolution of the eastern Mediterranean. Geol. Soc. Lond. Spec. Publ. 17: 1–74.

Rosenbaum, G.; Lister, G. S.; and Duboz, C. 2002. Relative motions of Africa, Iberia and Europe during Alpine orogeny. Tectonophysics 359:117–129.

Şengör, A. M. C., and Yılmaz, Y. 1981. Tethyan evolution of Turkey: a plate tectonic approach. Tectonophysics 75:181–241.

Seymen, I. 1981. Stratigraphy and metamorphism of the Kırşehir massif around Kaman. Geol. Bull. Turk. 24: 101–108 (in Turkish).

Simpson, C. 1985. Deformation of granitic rocks across the brittle-ductile transition. J. Struct. Geol. 7:503–511.

Snoke, A.; Tullis, J.; and Todd, V. R. 1998. Fault-related rocks: a photographic atlas. Princeton, NJ, Princeton University Press, 617 p.

Stampfli, G. M.; Mosar, J.; Marquer, D.; Marchant, R.; Baudin, T.; and Borel, G. 1998. Subduction and obduction processes in the Swiss Alps. Tectonophysics 296: 159–204.

Steiger, R. H., and Jager, E. 1977. Subcommission on geochronology: convention on the use of decay constants in geo- and cosmochronology. Earth Planet. Sci. Lett. 36:359–362.

Tatar, S., and Boztuğ, D. 1998. Fractional crystallization and magma mingling/mixing processes in the Monzonitic association in the SW part of the composite Yozgat batholith (Şefaatli-Yerköy, SW Yozgat). Turk. J. Earth Sci. 7:215–230.

———. 2005. The syn-collisional Danacıobası biotite leucogranite derived from the crustal thickening in central Anatolia (Kırıkkale), Turkey. Geol. J. 40:571–591.

Tatar, S.; Boztuğ, D.; Harlavan, Y.; and Arehart, G. B. 2003. The composite Behrekdağ batholith: an igneous record for the collision between Anatolides and Pontides along Izmir-Ankara-Erzincan Zone around Kırıkkale region, central Anatolia, Turkey. Abstract *in* 56th Geological Congress of Turkey, Proc., Ankara, p. 28–31.

Tullis, J., and Yund, R. A. 1985. Dynamic recrystallization of feldspar: a mechanism for ductile shear zone formation. Geology 13:238–241.

———. 1991. Diffusion creep in feldspar aggregates: experimental evidence. J. Struct. Geol. 13:987–1000.

Tüysüz, O.; Dellaloğlu, A. A.; and Terzioğlu, N. 1995. A magmatic belt within the Neo-Tethyan suture zone and its role in the tectonic evolution of northern Turkey. Tectonophysics 243:173–191.

Wang, Y.; Zhang, X.; Sun, L.; and Wan, J. 2007. Cooling history and tectonic exhumation stages of the south-central Tibetan plateau (China): constrained by $^{40}Ar/^{39}Ar$ and apatite fission track thermochronology. J. Asian Earth Sci. 29:266–282.

Wang, Z. H., and Lu, H. F. 2000. Ductile deformation and $^{40}Ar/^{39}Ar$ dating of the Changle-Nanao ductile shear zone, southeastern China. J. Struct. Geol. 22:561–570.

West, D. P., Jr., and Lux, D. R. 1993. Dating mylonitic deformation by the $^{40}Ar/^{39}Ar$ method: an example from the Norumbega fault zone, Maine. Earth Planet. Sci. Lett. 120:221–237.

Whitney, D. L., and Dilek, Y. 1997. Core complex development in central Anatolia. Geology 25:1023–1026.

Whitney, D. L., and Hamilton, M. A. 2004. Timing of high-grade metamorphism in central Turkey and the assembly of Anatolia. J. Geol. Soc. Lond. 161:1–6.

Whitney, D. L.; Teyssier, C.; Dilek, Y.; and Fayon, A. K. 2001. Metamorphism of the central Anatolian crystalline complex, Turkey: influence of orogen-normal collision vs. wrench-dominated tectonics on P-T-t paths. J. Metamorph. Geol. 19:411–432.

Whitney, D. L.; Teyssier, C.; Fayon, A. K.; Hamilton, M. A.; and Heizler, M. J. 2003. Tectonic controls on metamorphism, partial melting, and intrusion: timing of regional metamorphism and magmatism of the Niğde Massif, Turkey. Tectonophysics 376:37–60.

Xu, B.; Grove, M.; Wang, C.; Zhang, L.; and Liu, S. 2000. $^{40}Ar/^{39}Ar$ thermochronology from the northwestern Dabie Shan: constraints on the evolution of Qinling-Dabie orogenic belt, east-central China. Tectonophysics 322:279–301.

Yalınız, K. M.; Aydın, N. S.; Göncüoğlu, M. C.; and Parlak, O. 1999. Terlemez quartz monzonite of central Anatolia (Aksaray-Sarikaman): age, petrogenesis and geotectonic implications for ophiolite emplacement. Geol. J. 34:233–242.

Yalınız, M. K.; Floyd, P. A.; and Göncüoğlu, M. C. 1996. Supra-subduction zone ophiolites of central Anatolia: geochemical evidence from the Sarıkaman ophiolite, Aksaray, Turkey. Miner. Mag. 60:697–710.

Yalınız, M. K., and Göncüoğlu, M. C. 1998. General geological characteristics and distribution of the central Anatolian ophiolites. Hacettepe Univ. Yerbilimleri Dergisi 20:19–30 (in Turkish).

York, D. 1969. Least squares fitting of a straight line with correlated errors. Earth Planet. Sci. Lett. 5:320–324.

Zegers, T. E.; Wijbrans, J. R.; and White, S. H. 1999. $^{40}Ar/^{39}Ar$ age constraints on tectonothermal events in the Shaw area of the eastern Pilbara granite-greenstone terrain (W Australia): 700 Ma of Archean tectonic evolution. Tectonophysics 311:45–81.